JCB Journal of Cell Biology

ARTICLE

ISM1 regulates NODAL signaling and asymmetric organ morphogenesis during development

Liliana Osório[1,2*], Xuewei Wu[1,2*], Linsheng Wang[1,2*], Zhixin Jiang[1,2], Carlos Neideck[1,2], Guojun Sheng[3,4], and Zhongjun Zhou[1,2]

Isthmin1 (ISM1) was originally identified as a fibroblast group factor expressed in *Xenopus laevis* embryonic brain, but its biological functions remain unclear. The spatiotemporal distribution of ISM1, with high expression in the anterior primitive streak of the chick embryo and the anterior mesendoderm of the mouse embryo, suggested that ISM1 may regulate signaling by the NODAL subfamily of TGB-β cytokines that control embryo patterning. We report that ISM1 is an inhibitor of NODAL signaling. ISM1 has little effect on TGF-β1, ACTIVIN-A, or BMP4 signaling but specifically inhibits NODAL-induced phosphorylation of SMAD2. In line with this observation, ectopic ISM1 causes defective left-right asymmetry and abnormal heart positioning in chick embryos. Mechanistically, ISM1 interacts with NODAL ligand and type I receptor ACVR1B through its AMOP domain, which compromises the NODAL–ACVR1B interaction and down-regulates phosphorylation of SMAD2. Therefore, we identify ISM1 as an extracellular antagonist of NODAL and reveal a negative regulatory mechanism that provides greater plasticity for the fine-tuning of NODAL signaling.

Introduction

The TGF-β superfamily includes a large number of secreted signaling factors that are essential for embryonic development, tissue homeostasis, and human diseases such as cancer (Wakefield and Hill, 2013). These factors are secreted as precursors that undergo activation through cleavage by proprotein convertases (Constam, 2014). Based on the structural and sequence similarities, members of the TGF-β superfamily are categorized into several subfamilies that include TGB-β, ACTIVIN, NODAL, growth differentiation factors (GDFs), and bone morphogenetic proteins (BMPs). NODAL was first described to be critical for embryonic development in mice (Zhou et al., 1993; Conlon et al., 1994; Collignon et al., 1996). Evolutionarily conserved from hydra to human (although absent from fly and worm), NODAL plays key roles in embryonic patterning, namely, the formation of both anterior-posterior (AP) and left-right (LR) body axes (Rossant and Tam, 2009). NODAL is also important for the maintenance of pluripotency of embryonic stem cells and germ layer specification (Shen, 2007). Increasing evidence suggests that the cooperation between NODAL and GDF ligands is involved in the embryonic development. NODAL-GDF1 heterodimers rather than NODAL homodimers are required for mesendoderm and endoderm formation (Tanaka et al., 2007; Fuerer et al., 2014; Montague and Schier, 2017), whereas GDF3 is an essential coligand for NODAL signaling in germ layer formation and LR patterning during early development (Levine et al., 2009; Peterson et al., 2013; Pelliccia et al., 2017). In addition to its roles in early embryogenesis, NODAL signaling has recently been reported to be involved in homeostasis of adult reproductive tissues (Park and Dufort, 2011; Park et al., 2012) and carcinogenesis (Kirsammer et al., 2014). NODAL binds to a coreceptor CRIPTO (also known as TDGF1) and a heterodimeric receptor complex composed of Activin receptor type IB (ACVRIB; also known as ALK4) and ACVRIIA/IIB. This triggers the phosphorylation of SMAD2/3, which is then transported into the nucleus, where it interacts with nuclear factors such as FOXH1 (also known as FAST2) to regulate the transcription of targeted genes (Schier, 2009).

Isthmin 1 (ISM1) was first identified in *Xenopus laevis* gastrula embryos by an unbiased secretion cloning screen (Pera et al., 2002). Named after its prominent expression location in the isthmus region of the brain, ISM1 was described as a member of the *FGF8* synexpression group. ISM1 has since been described as a target of WNT/β-Catenin and NODAL signaling in the zebrafish embryo (Weidinger et al., 2005; Bennett et al., 2007). In the chick embryo, ISM1 is among the top 20 genes expressed in the anterior primitive streak (Alev et al., 2010), a fundamental

[1]School of Biomedical Sciences, Li Ka Shing Faculty of Medicine, The University of Hong Kong, Hong Kong; [2]Shenzhen Institute of Innovation and Research, The University of Hong Kong, Nanshan, Shenzhen, China; [3]International Research Center for Medical Sciences, Kumamoto University, Kumamoto, Japan; [4]RIKEN Center for Developmental Biology, Kobe, Japan.

*L. Osório, X. Wu, and L. Wang contributed equally to this paper; Correspondence to Zhongjun Zhou: zhongjun@hku.hk.

structure of the embryo whose formation marks the start of gastrulation and germ layer formation. Despite this information, the biological function of ISM1 remains largely unexplored. ISM1 has been reported as an angiogenesis inhibitor during tumor progression (Xiang et al., 2011) that has a dual function in endothelial cell survival and apoptosis through cell surface receptors αVβ5 integrin (Zhang et al., 2011) and GRP78 (Chen et al., 2014). Based on its spatiotemporal distribution throughout mouse ontogeny (Osório et al., 2014), we speculate that ISM1 is likely to function as more than an angiogenesis inhibitor. Present in the embryo as early as embryonic day 6.75 in the anterior mesendoderm, ISM1 is dynamically expressed in several of its derivatives, such as paraxial mesoderm, lateral plate mesoderm (LPM), and endoderm. Since its expression persists in several adult tissues, ISM1 seems to be involved not only in embryogenesis but also in organ homeostasis. The sparse information available on ISM1 led us to search for a cue of its putative function based on its distinct structural features. The ISM protein family is characterized by the presence of thrombospondin type 1 repeat (TSR1) and an AMOP (adhesion-associated domain in MUC4 and other proteins) domain. While TSR1 is well characterized and present in many extracellular proteins (Tucker, 2004), AMOP is found only in MUC4, SUSD2, ISM1, and ISM2, with little-known functions (Ciccarelli et al., 2002). Several functions have been attributed to the TSR1 domain, among which is the ability to activate and regulate TGF-β signaling (Adams and Lawler, 2011). We therefore tested the potential involvement of ISM1 in TGF-β superfamily pathway signaling.

Results

ISM1 is a secreted soluble *N*-glycosylated protein

Similar to its counterpart in *Xenopus*, mouse ISM1 is a secreted protein that, when ectopically expressed in HEK293T cells, is detected as a single band of ∼70 kD in both whole-cell lysates (WCLs) and conditioned medium (CM) samples (Fig. 1 A). Since the molecular weight of the detected ISM1 was larger than expected (52 kD), ISM1 is likely subject to posttranslational modifications. Glycosylation is commonly found in many secreted proteins (Moremen et al., 2012), and analysis of the ISM1 protein sequence predicted two putative *N*-glycosylation sites at positions N39 and N282 (Osório et al., 2014; see Fig. 6 A). Indeed, biochemical analyses showed that ISM1 is an *N*-glycosylated protein. PNGase F treatment reduced ISM1 molecular weight in both WCL and CM, whereas endoglycosidase H (Endo H) treatment reduced ISM1 MW only in WCL (Fig. 1 A). As PNGase F digestion removes almost all types of *N*-linked (Asn-linked) glycosylation while Endo H predominantly removes high-mannose *N*-glycans, this result suggests that intracellular ISM1 contains predominantly oligomannose *N*-glycans, whereas secreted ISM1 contains a more complex type of *N*-glycans. Glycosylation of ISM1 was further confirmed by mutating asparagine residues to glutamine at each single position (N39Q or N282Q) or in combination (N39Q/N282Q), which led to a shift of the intracellular ISM1 MW from 70 kD to ∼65 kD and 60 kD, respectively (Fig. 1 B). Mutant ISM1 (N39Q/N282Q) was no longer sensitive to PNGase F treatment, indicating that both N39

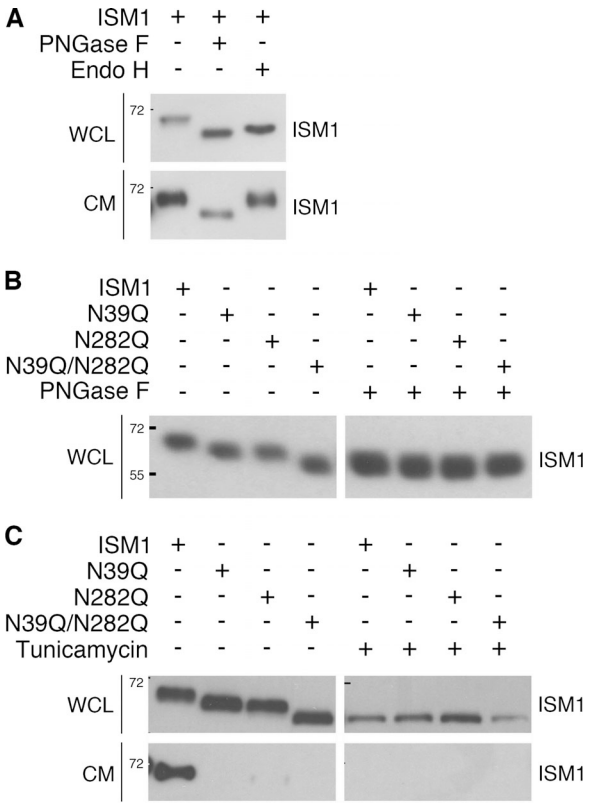

Figure 1. **Mouse ISM1 is a secreted soluble protein that is glycosylated at asparagine residues 39 and 282. (A)** Western blot of ISM1 in WCL and CM samples of HEK293T cells transiently transfected with mouse ISM1 and digested with PNGase F or Endo H as indicated. ISM1 protein is detected as a band of ∼70 kD in both WCL and CM without digestion. **(B)** HEK293T cells were transiently transfected with ISM1 or its N39Q, N282Q, and N39Q/N282Q point mutated forms. WCL samples were digested with or without PNGase F and subjected to Western blotting to detect ISM1. The size of intracellular ISM1 shifted from 70 kD to ∼65 and 60 kD following single or combined N point mutations, respectively. **(C)** Western blot of ISM1 in WCL and CM samples of HEK293T cells transiently transfected with wild-type ISM1 or its N39Q, N282Q, and N39Q/N282Q point mutated forms, in the presence or absence of 1 ng/ml tunicamycin. The protein molecular weight markers in kilodaltons are indicated by numbers on the left side of the Western blots.

and N282 residues are *N*-glycosylated. Treatment of cells expressing either ISM1 or its asparagine residue mutant forms with tunicamycin, an inhibitor of *N*-glycosylation, led to similar changes in ISM1 migration (Fig. 1 C), further supporting that ISM1 is *N*-glycosylated. *N*-glycosylation in ISM1 is essential for its secretion, as eliminating glycosylation, by either point mutations or tunicamycin treatment, dramatically reduced the amount of ISM1 in the CM (Fig. 1 C). These data provided the first experimental evidence that ISM1 is *N*-glycosylated at both N39 and N282 residues and that this modification is essential for its secretion.

ISM1 is an extracellular antagonist of the NODAL signaling pathway

The TSR1 domain is well known for its involvement in the regulation of TGF-β signaling (Adams and Lawler, 2011). We therefore asked if ISM1 regulates the TGF-β superfamily

signaling pathway. To test our hypothesis, we examined whether ISM1 has any effect on SMAD activation mediated by the major ligands of the TGF-β superfamily, including TGF-β, ACTIVIN, and NODAL, using the CM collected from HEK293T cells ectopically expressing ISM1. While TGF-β, ACTIVIN, and NODAL signals are largely transduced through the phosphorylation of SMAD2/3, BMPs activate SMAD1/5/8. We found no significant changes in phosphorylated SMAD2 (pSMAD2) levels in the presence or absence of ISM1 CM, in response to the stimulation of either TGF-β1 or ACTIVIN-A (Fig. 2 A). However, CM containing ISM1 led to a significant reduction in SMAD2 phosphorylation elicited by NODAL (Fig. 2 B). A similar observation was found in the presence of GDF1, a NODAL-related TGF-β ligand that uses the same core components of the signaling pathway (Shen, 2007; Schier, 2009) and forms NODAL–GDF1 heterodimers (Tanaka et al., 2007; Fuerer et al., 2014; Montague and Schier, 2017; Fig. 2 B). On the other hand, in response to BMP4, no obvious alteration in pSMAD1/5/8 levels was observed between ISM1 CM treatment and mock CM treatment (Fig. 2 C). These results indicate that ISM1 modulates SMAD-mediated TGF-β superfamily signaling in a ligand-dependent manner. This was further confirmed by purified recombinant mouse ISM1 protein (Fig. 2, D and E). The antagonizing effect on NODAL signaling by ISM1 was further examined on the transcription of SMAD2 downstream targeted genes. One of the best understood SMAD2 targets is *Mix.2* gene (Chen et al., 1996, 1997; Liu et al., 1997). In the nucleus, pSMAD2 associates with FOXH1 to form a transcriptional complex on the ACTIVIN-NODAL-TGF-β responsive element of the *Mix.2* promoter. Its activity can be measured by the *A3-luc* reporter gene assay, which has been extensively used as "readout" of the NODAL signaling pathway (Liu et al., 1997; Iratni et al., 2002; Yan et al., 2002; Gray et al., 2003; Chen and Shen, 2004; Cheng et al., 2004). Consistent with the results on SMAD2 phosphorylation, both recombinant ISM1 (rISM1) and ISM1 CM inhibited SMAD2/FOXH1 transcriptional activity induced by NODAL (Fig. 3, A and B). In addition, the NODAL signaling antagonism by ISM1 was dose dependent in the *A3-luc* reporter gene assay, with stronger inhibitory effects at higher ISM1 concentrations (Fig. 3, A and B). However, ISM1 CM did not significantly impact the SMAD2/FOXH1 transcriptional activity induced by either TGF-β1 or ACTIVIN-A (Fig. 3, C and D). These results suggest that ISM1, acting as a secreted protein, specifically antagonizes NODAL signaling, leading to reduced activation of its major intracellular effector SMAD2 and decreased SMAD2/FOXH1 transcriptional activity. In addition to *Mix.2*, several other genes have been reported, including *NODAL* gene itself, to be NODAL targets (Shen, 2007; Schier, 2009). In chick embryos, it has been shown that NODAL-soaked beads induce ectopic expression of *NODAL* in ∼50% of embryos when implanted in the right side of the embryo (Schlueter and Brand, 2009). To test the inhibitory effect of ISM1 on NODAL signaling in vivo, we used the same assay to examine how ISM1 affects the ability of NODAL to regulate its own expression (Fig. 3 E). As shown in Fig. 3 (F and G), 58% of embryos (7 of 12) implanted with rNODAL + PBS beads showed ectopic *NODAL* expression in the right LPM, whereas ectopic *NODAL* expression was detectable in only 14% of embryos (2 of 14) implanted with rNODAL + rISM1 beads. Taken together, these results are in agreement with our previous observations and identify ISM1 as a new extracellular antagonist of the NODAL signaling pathway.

Magnitude of inhibition of NODAL signaling by ISM1, LEFTY1, and CER1

At present, the LEFTY and DAN/CER families of proteins are known extracellular antagonists of NODAL signaling (Shen, 2007; Schier, 2009). LEFTY1 and 2 are divergent noncanonical TGF-β ligands that, often through a negative-feedback mechanism (Meno et al., 1998, 1999; Branford and Yost, 2002; Feldman et al., 2002), block NODAL signaling by binding to NODAL itself and its coreceptor CRIPTO (Chen and Shen, 2004; Cheng et al., 2004). Members of the DAN/CER family are cysteine-rich extracellular proteins that inhibit NODAL signaling through their direct interaction with NODAL ligand (Piccolo et al., 1999; Perea-Gomez et al., 2002; Marques et al., 2004). To compare the inhibitory effect of ISM1 on NODAL signaling with known extracellular antagonists, ectopic FLAG-tagged LEFTY1, FLAG-tagged ISM1, and FLAG-tagged CER1 were expressed in HEK293T. CM was collected from these cells individually for the evaluation. NODAL signaling was examined in HEK293T-CRIPTO cells by Western blotting of pSMAD2 upon NODAL stimulation in the presence of LEFTY1, ISM1, or CER1. As shown in Fig. 4 (A and B), NODAL treatment readily activated SMAD2, represented by a significant elevated phosphorylation of SMAD2. LEFTY1, ISM1, and CER1 all caused a significant decrease in pSMAD2 levels in a dose-dependent manner. Similar dose-dependent inhibitory effects for LEFTY1, ISM1, and CER1 on SMAD2/FOXH1 transcriptional activity were observed in the *A3-luc* luciferase reporter activity assay (Fig. 4 C). In both sets of experiments, LEFTY1 exhibited the strongest inhibition to NODAL signaling and almost completely abolished pSMAD2 (∼90% of reduction) at higher concentrations, whereas the inhibition to NODAL signaling by CER1 was much weaker (∼40% of reduction at similar concentrations; Fig. 4, A–C). These observations are in line with the previous report showing CER1 as a potent antagonist of NODAL signaling (Meno et al., 1999). Compared with CER1, similar or lower concentrations of ISM1 (determined by Western blotting using anti-FLAG antibodies) could achieve comparable (*A3-luc* luciferase reporter activity assay) or slightly stronger (pSMAD2 level) inhibition to NODAL signaling (Fig. 4, A–C). In the presence of undiluted ISM1 CM, pSMAD2 levels and SMAD2/FOXH1 transcriptional activity are reduced to ∼40 and ∼60%, respectively (Fig. 4, A–C). Taken together, these comparative analyses of NODAL signaling inhibition, at the level of both SMAD2 activation and its subsequent transcriptional activity, revealed that ISM1 is an antagonist of NODAL signaling with a similar inhibitory activity to CER1.

ISM1 interacts with NODAL ligand and type I receptor ACVR1B

To understand the molecular mechanism underlying the inhibitory effect of ISM1 on NODAL signaling, we examined the potential interaction between ISM1 and the distinct components of the NODAL signaling pathway through a series of ligand-binding assays. As shown in Fig. 5 A, ISM1 was found to interact with

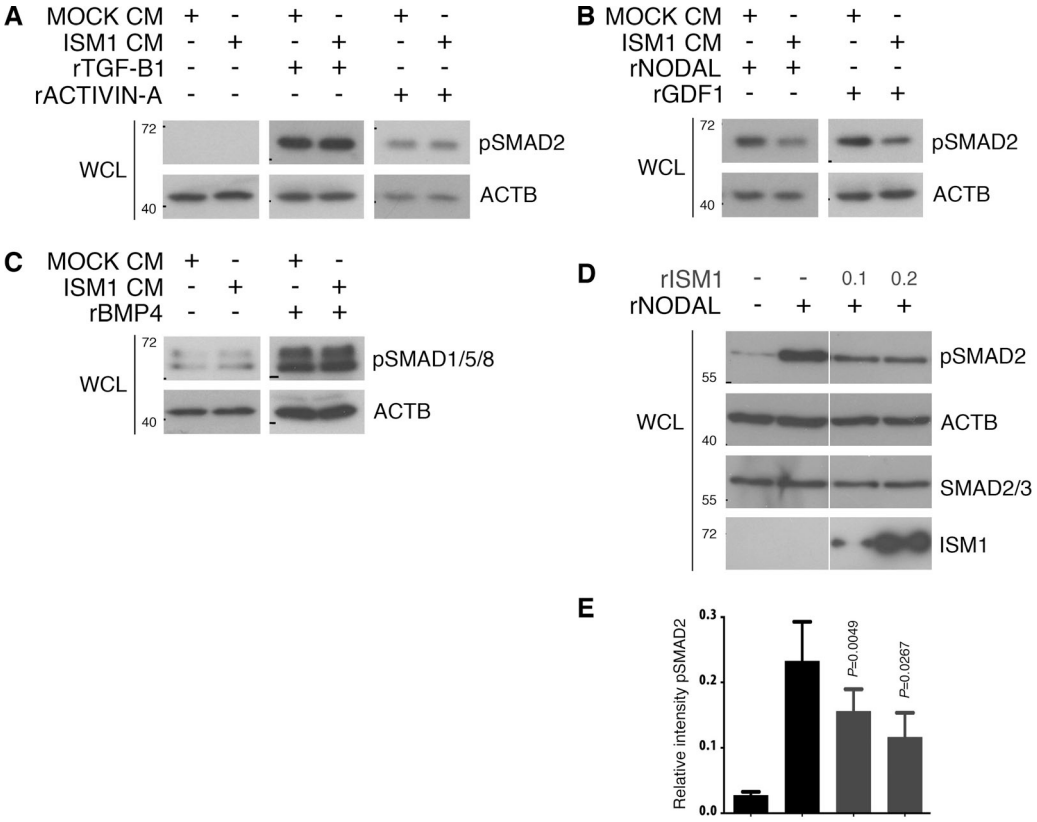

Figure 2. **ISM1 modulates R-SMAD activation by members of the TGF-β superfamily in a ligand-dependent manner. (A)** Western blot of pSMAD2 in WCL of serum-starved HEK293T cells treated with 40 ng/ml TGF-β1 or 40 ng/ml ACTIVIN-A in the presence of mock or ISM1 CM. For each panel, two biological replicates were performed. **(B)** Western blot of pSMAD2 in WCL of serum-starved HEK293T-CRIPTO cells treated with 100 ng/ml NODAL or 100 ng/ml GDF1 in the presence or absence of ISM1 CM as indicated. For each panel, two biological replicates were performed. **(C)** Western blot of pSMAD1/5/8 in WCL of serum-starved HEK293T cells treated with 50 ng/ml BMP4 in the presence or absence of ISM1 CM. For each panel, two biological replicates were performed. **(D)** Western blot of pSMAD2 in WCL of serum-starved HEK293T-CRIPTO cells treated with 100 ng/ml NODAL in the presence of 0, 100, or 200 ng/ml ISM1 protein. **(E)** Quantification of the intensity of pSMAD2 relative to β-actin in three biological replicates. The protein molecular weights in kilodaltons are indicated by numbers on the left side of the Western blots. Data represent mean ± SEM. ACTB, β-actin.

both the proprotein and mature forms of NODAL ligand in the CM. GST pull-down assays and surface plasmon resonance (SPR)–based interaction analysis further confirmed the direct interaction between ISM1 and NODAL ligand (Fig. S1). We then tested whether ISM1 interacts with the receptor complex by an in situ proximity ligation assay (PLA). As shown in Fig. 5 B, significantly higher numbers and percentages of PLA$^+$ signals were found in ACVR1B-transfected cells treated with ISM1 CM, compared with those treated with mock CM, suggesting that ISM1 could form a complex with ACVR1B. Since ISM1 acts as a secreted protein, we hypothesize that its interaction with the receptor complex is likely to occur through their extracellular domains. To test this hypothesis, we generated soluble forms of the N-terminal ectodomain (ECD) of ACVR1B and ACVR2B (ACVR1B^{ECD} and ACVR2B^{ECD}; Fig. 5 C) that allowed us to discriminate which particular element of the receptor complex is involved in the interaction. We found that ISM1 interacted with ACVR1B^{ECD} in a cell-independent manner (Fig. 5 D). GST pull-down assays and SPR-based interaction analysis further confirmed the direct interaction between ISM1 and ACVR1B ligand (Fig. S1). In contrast, no interaction between ISM1 and ACVR2B^{ECD} (Fig. 5 E) or between ISM1 and the coreceptor CRIPTO was observed (Fig. 5 F). As ACVR2A has been shown to interact with NODAL (Kelber et al., 2008; Wang et al., 2016), we then tested if ISM1 could also interact with ACVR2A. As shown in Fig. S2, coimmunoprecipitation experiments indicated interaction between ISM1 and ACVR2A. These data suggested that ISM1 could bind intimately to both ligand and receptor complex components of NODAL signaling.

Inhibition of NODAL signaling by ISM1 requires the AMOP domain

To understand which domain of ISM1 mediates the interaction with components of the NODAL signaling pathway, we generated domain-deleted ISM1 constructs lacking either TSR1 (ΔTSR1) or AMOP (ΔAMOP) domains (Fig. 6 A). The boundaries for TSR1 and AMOP domains have been previously described (Osório et al., 2014): TSR1 domain spans amino acids 215–259, and AMOP domain spans amino acids 286–449. While ISM1 expression is not affected by the absence of either domain, several bands were detected in WCL samples of ISM1 lacking AMOP (Fig. 6 B). Treatment with PNGase F or Endo H eliminated the higher-molecular weight bands, suggesting that these correspond to different *N*-glycosylated

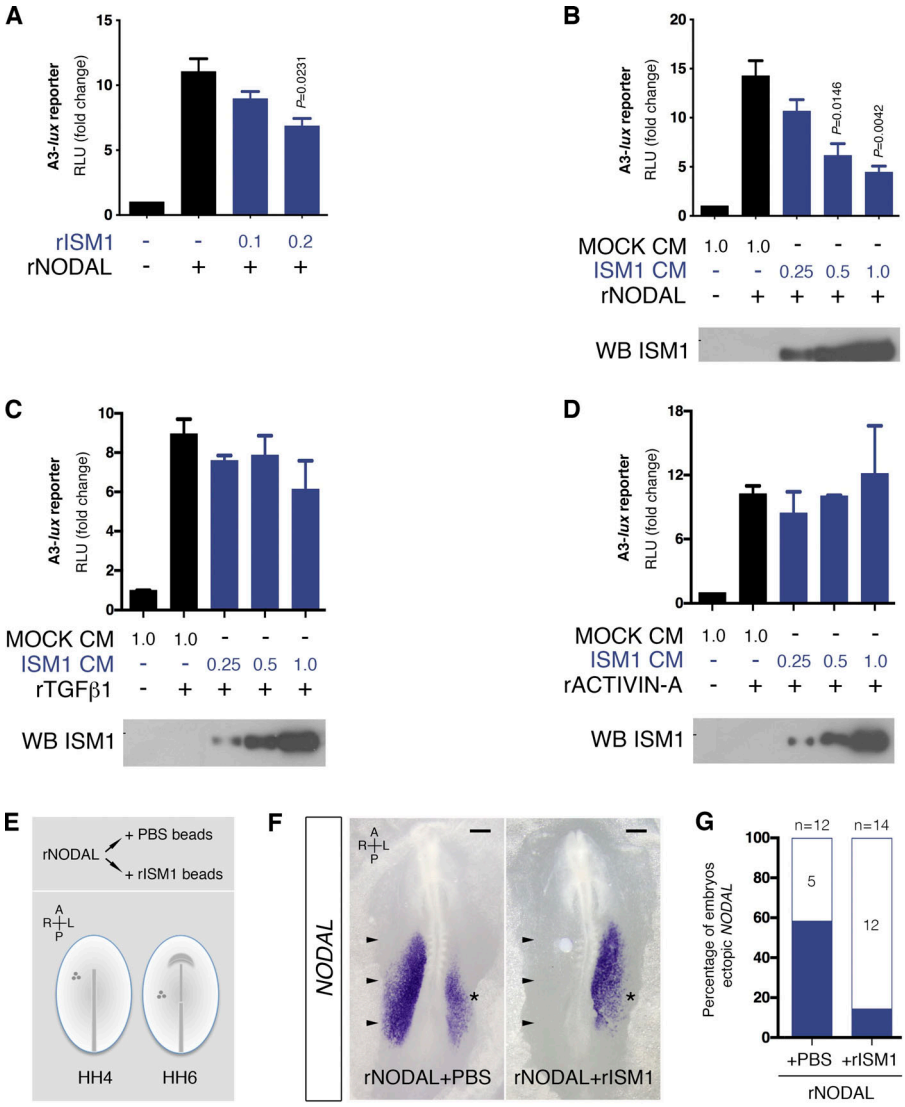

Figure 3. **Effect of ISM1 on SMAD2/FOXH1 transcriptional activity and gene expression of NODAL downstream targets. (A)** Fold changes of SMAD2/FOXH1 transcriptional activity represented by relative luciferase units (RLU) in serum-starved HEK293T-CRIPTO cells treated with 100 ng/ml NODAL in the presence of 0, 100, or 200 ng/ml of rISM1 protein. Data from three independent experiments of dual luciferase reporter assay. **(B)** NODAL-induced transcriptional activity of SMAD2/FOXH1 in serum-starved HEK293T-CRIPTO cells in the presence of mock or increasing doses of ISM1 CM. The dosage of CM used is represented by the percentage of CM in the culture medium. Data from three independent experiments. Relative ISM1 protein levels in each treatment are shown by Western blot (WB). **(C and D)** Fold change of transcription of *A3-luc* reporter represented by RLU in serum-starved HEK293T cells treated with 40 ng/ml TGF-β1 (C) or 40 ng/ml ACTIVIN-A (D) in the presence of mock or increasing doses of ISM1 CM. Data from three independent experiments. Relative ISM1 protein levels in each treatment are shown by Western blot. Data represent mean ± SEM; statistical analyses were performed using unpaired, two-tailed *t* test, and statistically significant P values are indicated. **(E)** Schematic diagram of the experimental approach to test the inhibitory effect of ISM1 in NODAL-induced *NODAL* gene expression in chick embryos. When implanted on the right side of embryos at stages HH4–6, NODAL-soaked beads induce ectopic *NODAL* expression. The ability of NODAL to induce its own expression was tested in the presence of purified mouse rISM1 protein in embryos cultured *ex ovo*. **(F)** *NODAL* whole-mount in situ hybridization in embryos implanted with rNODAL + PBS– or rNODAL + rISM1–soaked beads. Arrowheads point to the ectopic *NODAL* expression in the right LPM, while asterisks indicate the endogenous *NODAL* expression on the left LPM. Embryos are shown in ventral view, and orientation along the AP and LR axes are indicated. Scale bar, 25 µm. **(G)** Percentage of embryos showing ectopic *NODAL* expression on the right LPM following implantation with beads soaked with rNODAL + PBS or rNODAL + rISM1.

forms of ISM1. In addition, deletion of TSR1 or AMOP domain does not affect *N*-glycosylation and secretion of ISM1 (Fig. 6 B). Ligand-binding experiments showed that AMOP domain is required for ISM1 interaction with the components of the NODAL signaling pathway, as the interactions between ISM1 and NODAL or ACVR1B were lost when AMOP domain was deleted. However, deletion of TSR1 domain in ISM1 did not significantly affect the interactions (Fig. 6, C and D). In line with this, the inhibition of NODAL-induced phosphorylation of SMAD2 by ISM1 was attenuated only when AMOP domain was deleted (Fig. 6 E). These results indicated that the inhibition of NODAL signaling by ISM1 is dependent on its AMOP domain, which mediates the physical interaction of ISM1 with NODAL and ACVR1B.

ISM1 compromises the formation of NODAL–ACVR1B complex

The interactions of ISM1 with NODAL, ACVR1B, and ACVR2A raise the possibility that ISM1 may disturb NODAL signaling through interfering with the interaction between NODAL ligand and receptor complex. To test if ISM1 could potentially prevent NODAL and/or ACVR1B interaction with the coreceptor CRIPTO, we performed competitive binding assays. As shown in Fig. 7 A, the interaction between NODAL and a soluble form of CRIPTO (sCRIPTO) was not disturbed by increasing concentrations of ISM1. Similarly, the interaction between sCRIPTO and ACVR1B^{ECD} also remained largely unchanged with increasing concentrations of ISM1 (Fig. 7 B). However, NODAL–ACVR1B interaction was significantly compromised by the presence of ISM1. In a cell-independent assay, the physical

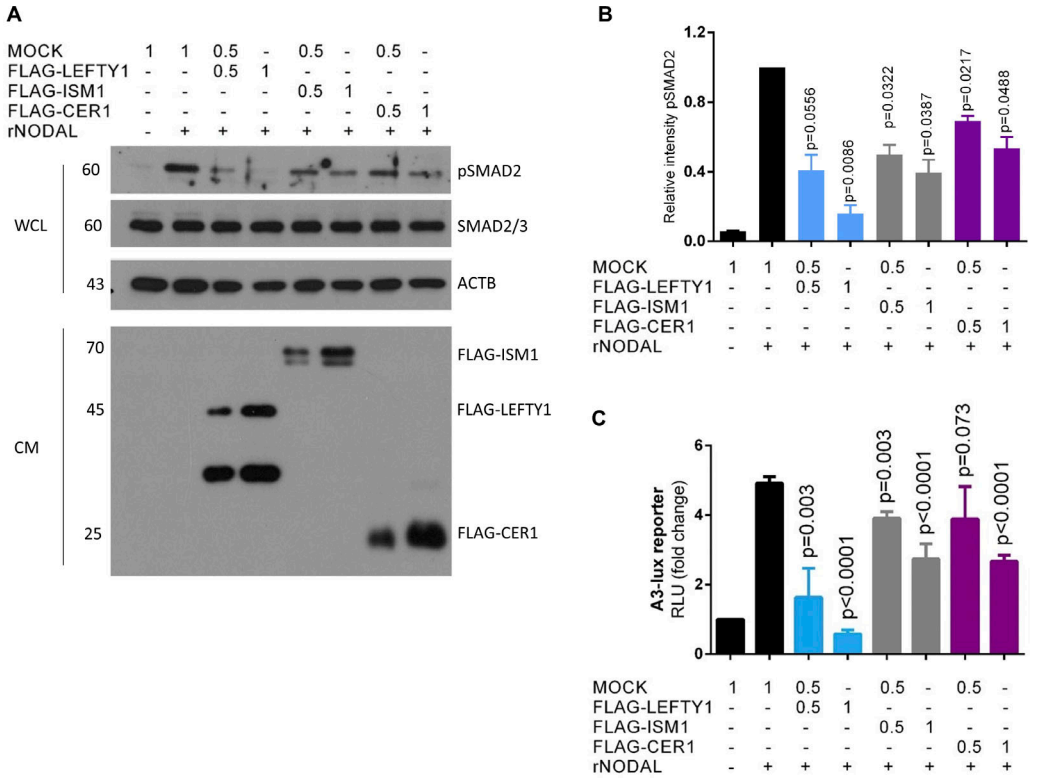

Figure 4. **The inhibitory effects of ISM1, LEFTY1, and CER1 on NODAL signaling. (A)** Serum-starved HEK293T-CRIPTO cells treated with 100 ng/ml rNODAL in the presence of mock, LEFTY1, ISM1, or CER1 CM at indicated dilutions. WCL samples were subjected to Western blotting analyses for pSMAD2. Total SMAD2/3 and β-actin were used as internal controls. The protein levels of LEFTY1, ISM1, and CER1 representing their relative concentrations in the CMs were analyzed by Western blotting using Flag antibodies. **(B)** Quantification of the intensity of pSMAD2 relative to SMAD2/3 in three biological replicates. Data represent mean ± SEM. The unpaired, two-tailed *t* test was used for statistical analyses. Statistically significant P values are indicated. **(C)** Dual luciferase reporter assay to determine the SMAD2/FOXH1 transcriptional activity in HEK293T-CRIPTO cells treated by 100 ng/ml rNODAL for 24 h, together with CM of mock, FLAG-LEFTY1, FLAG-ISM1, or FLAG-CER1 at the indicated dilutions. Data represent mean ± SEM of four independent experiments. P values of statistical analyses using unpaired, two-tailed *t* test are indicated in each individual experimental group.

interaction between NODAL and ACVR1B^{ECD} was greatly reduced by ISM1 CM in a dose-dependent manner (Fig. 7 C). In line with this result, NODAL–ACVR1B complex formation represented by PLA^{+} signals was significantly disturbed in the presence of ISM1 CM compared with mock CM (Fig. 7 D). On the other hand, the interaction between NODAL and ACVR2A was not disturbed in the presence of increasing concentrations of ISM1 (Fig. S3). These data provided strong evidence that ISM1 impacts the interaction between NODAL ligand and its receptor complex by specifically compromising NODAL–ACVR1B interaction.

ISM1 causes defective LR patterning in the chick embryo

NODAL signaling has a conserved role in the generation of LR asymmetry (Nakamura and Hamada, 2012; Grimes and Burdine, 2017). LR asymmetry is initiated in the node region during gastrulation and subsequently transmitted to the LPM. The asymmetric expression of *NODAL* in the left LPM, which depends on NODAL signaling itself, initiates a left-sided regulatory genetic cascade that involves downstream targets such as *CER1* and *PITX2* and that ultimately controls the shape and position of the internal organs. Our previous study (Osório et al., 2014) showed that ISM1 mRNA is asymmetrically distributed in the anterior mesendoderm of E7.5 mouse embryos and in the foregut endoderm of Hamburger and Hamilton stage 10 (HH10; Hamburger and Hamilton, 1951) chicks, suggesting that ISM1 may be potentially involved in LR asymmetric organ morphogenesis. We therefore explored the biological relevance of ISM1 as an antagonist of NODAL signaling during LR asymmetry. To address this question, we used the chick embryo assay in which embryos at HH4–5 were cultured *ex ovo* in the presence or absence of ISM1 CM. To test if ISM1 disturbs the left-sided gene expression downstream of NODAL signaling, we examined *NODAL* expression by whole-mount in situ hybridization, given that the *NODAL* gene itself is a downstream target of NODAL signaling. As shown in Fig. 8 (A and B), 87% of mock-treated embryos (21 of 24) exhibited strong expression of *NODAL* asymmetrically in the left LPM. In contrast, asymmetric expression of *NODAL* gene was observed in only 60% of ISM1-treated embryos (18 of 30). By quantitative real-time PCR (qPCR) analyses, *NODAL* relative transcription was significantly reduced by ∼70% in the left side of LPM in ISM1 CM–treated embryos (Fig. 8 C). In addition, the expression of other NODAL downstream targets was also disturbed by ISM1. As shown in Fig. 8 (D and E), 89% of mock-treated embryos (23 of 26) exhibited asymmetric *CER1* expression on the left side of LPM

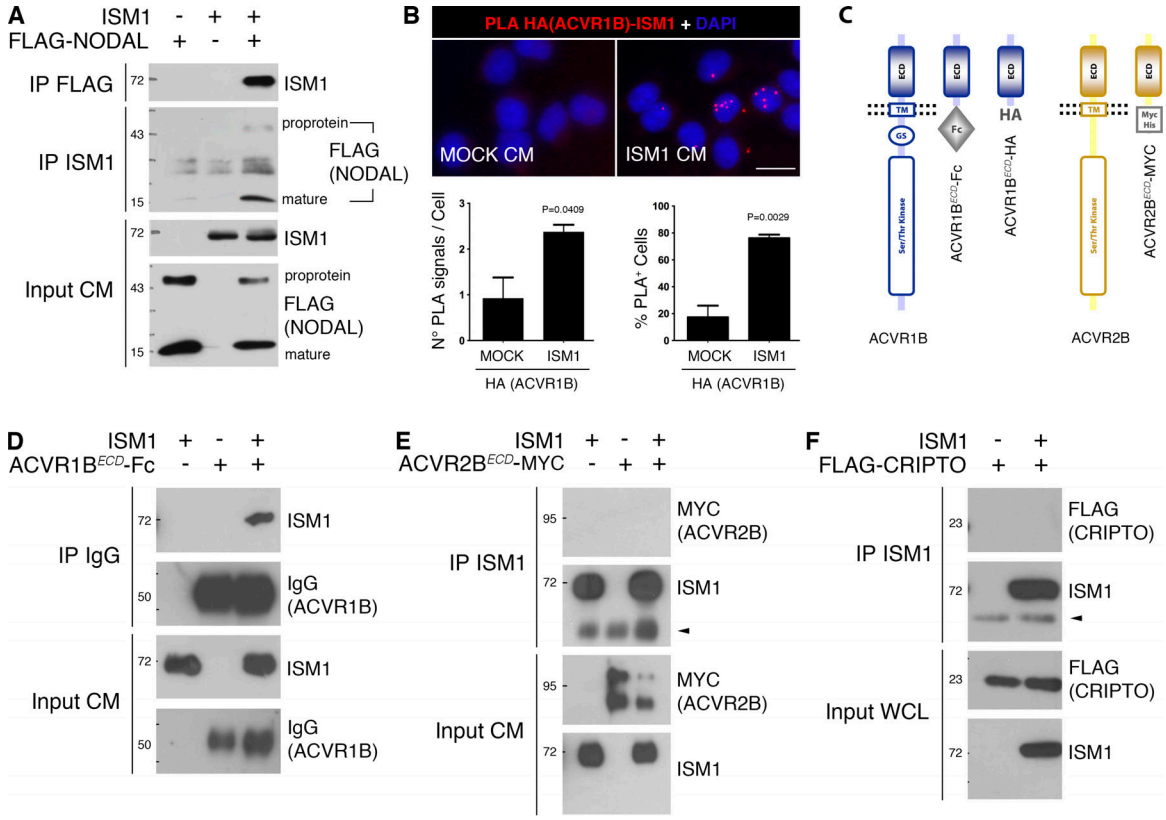

Figure 5. **Interaction of ISM1 with NODAL ligand and its type I receptor ACVR1B. (A)** HEK293T-CRIPTO cells were transiently transfected with ISM1 and FLAG-NODAL as indicated. CM samples were immunoprecipitated (IP) with anti-FLAG or anti-ISM1 antibodies and subjected to Western blot using antibodies against ISM1 and FLAG, respectively. Both precursor and mature forms of NODAL were pulled down from CM. **(B)** In situ PLA to detect ACVR1B-ISM1 complexes (red dots) in HeLa cells transiently expressing ACVR1B-HA plasmid at low dosage, in the presence or absence of ISM1 CM. Cells were counterstained with DAPI to visualize nuclei. The number of PLA signals per cell (lower left) and the percentage of cells that have PLA signals (lower right) were counted in a total of 200 cells. Scale bars, 20 µm. Data represent mean ± SEM. The unpaired, two-tailed *t* test was used for statistical analysis. **(C)** Schematic representation of the soluble forms of the ECD of ACVR1B and ACVR2B. ACVR1B^{ECD} was fused to either the HA epitope or to human IgG Fc fragment. ACVR2B^{ECD} was fused to MYC/His epitope. **(D)** HEK293T were transiently transfected with ISM1 and ACVR1B^{ECD}-Fc as indicated. CM samples were immunoprecipitated with protein G agarose beads and immunoblotted with anti-ISM1 and anti-IgG antibodies. **(E)** HEK293T were transiently transfected with ISM1 and ACVR2B^{ECD}-MYC as indicated. CM samples were immunoprecipitated with anti-ISM1 antibodies and subjected to Western blot with anti-MYC and anti-ISM1 antibodies. **(F)** WCL of HEK293T-CRIPTO cells transiently transfected with mock or ISM1 plasmids were precipitated with anti-ISM1 antibodies and analyzed by Western blot with antibodies against FLAG and ISM1. Arrowheads in E and F indicate the heavy chain of the IgG (50 kD). Protein molecular weight in kilodaltons is indicated by numbers on the left side of Western blots.

compared with only 67% (22 of 33) in ISM1-treated embryos. Moreover, the relative transcriptional levels of *CER1* and *PITX2* were significantly reduced in the left side of LPM in ISM1 CM–treated embryos (Fig. 8, F and G).

LEFTY1 is another NODAL target gene that has important functions in LR asymmetry, as it prevents NODAL signals from crossing to the right side of the embryo. In contrast to *CER1* and *PITX2*, we observed no obvious differences in *LEFTY1* expression along the midline between embryos treated with mock and ISM1 CM (Fig. 8, H and I), suggesting that *LEFTY1* is regulated by signals other than NODAL. This is in agreement with midline LEFTY1 being regulated by at least two parallel pathways involving NODAL and BMP (Yamamoto et al., 2003; Smith et al., 2011). To test if disrupted NODAL signaling in left LPM leads to defective organ asymmetry, we examined the direction of the heart looping, the first overt morphological asymmetry in the embryo. In mock-treated embryos, ∼88% embryos (36 of 41) manifested the correct heart position to the right side, whereas in ISM1-treated embryos, 56% (33 of 59) exhibited normal heart position (Fig. 8 J).Taken together, these data show that treatment of embryos with ISM1 results in defective NODAL signaling in the left LPM and impaired asymmetric heart morphogenesis. Acting in concert with the left-sided NODAL signaling, the existence of a right-sided signaling pathway that provides right identity to the organs has been recently proposed (Schlueter and Brand, 2009; Ocaña et al., 2017). BMP and fibroblast growth factor signals, operating on the right side of the embryo, activate downstream target genes such as SNAI1. When treated with ISM1 CM, embryos show no obvious differences in SNAI1 expression (Fig. 8, K and L), indicating that the observed LR asymmetry defects caused by ISM1 were not attributable to the perturbation of the right-specific signaling. Taken together, these results provide the first evidence of the biological relevance of ISM1 as an antagonist of NODAL signaling in asymmetric organ morphogenesis.

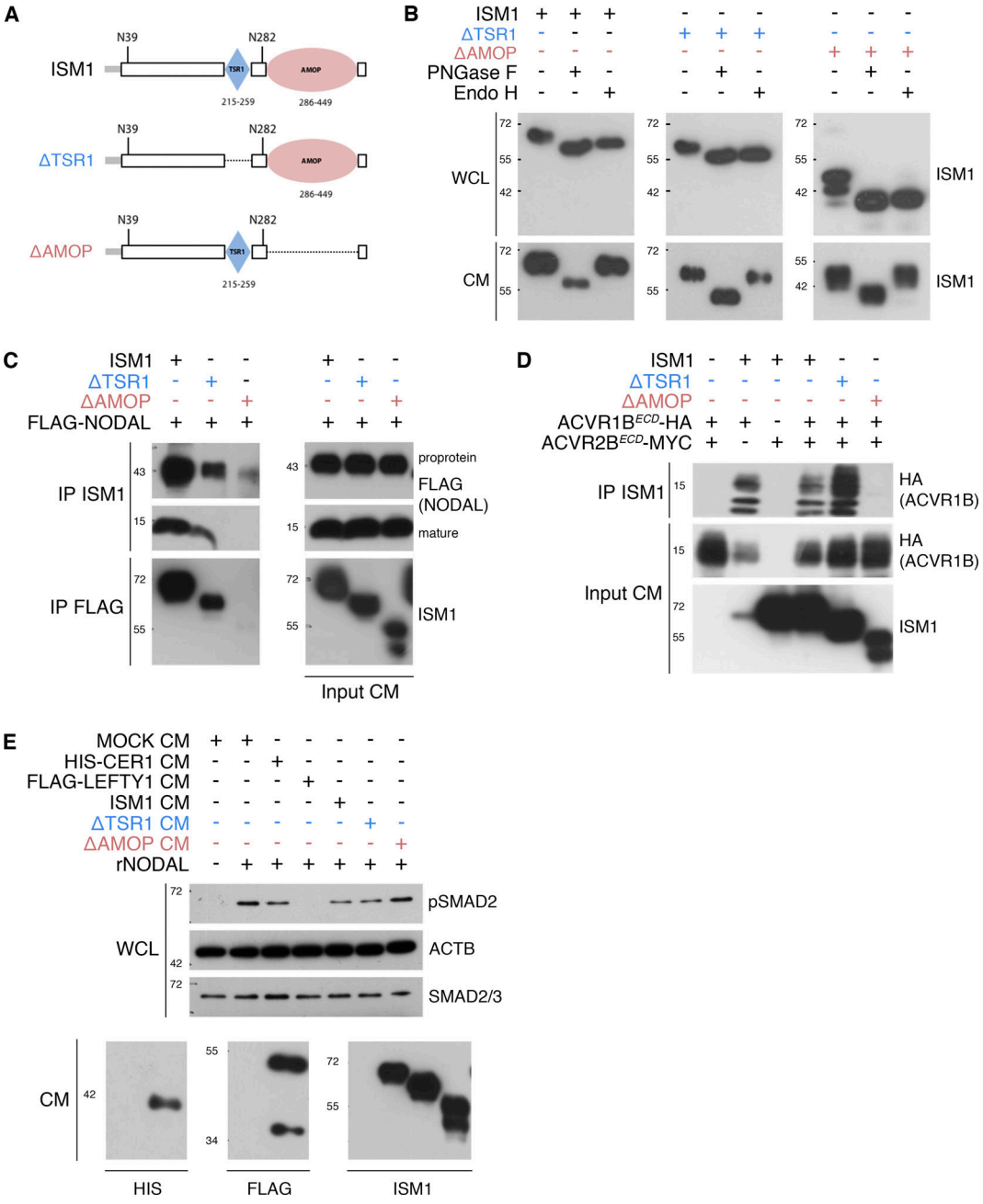

Figure 6. **AMOP domain is required for the function of ISM1 as an antagonist of NODAL signaling. (A)** Diagram of domain-deleted ISM1 constructs lacking either TSR1 or AMOP (ΔTSR1 and ΔAMOP, respectively). The *N*-glycosylation sites at positions N39 and N282 are indicated. N39 is located in the N terminus, 10 amino acids downstream from the signal peptide (amino acids 1–29), and N282 is located in the region between TSR1 and AMOP domains (amino acids 260–285). **(B)** Western blot of ISM1 in WCL and CM samples of HEK293T cells transiently transfected with wild-type ISM1, ΔTSR1-ISM1, or ΔAMOP-ISM1. Samples were digested with PNGase F or Endo H before being subjected to Western blotting. **(C)** Mapping of NODAL-interacting domain of ISM1. HEK293T cells were transiently transfected with FLAG-NODAL together with either wild-type ISM1 or domain-deleted ISM1 mutants. CM samples were immunoprecipitated (IP) with anti-FLAG or anti-ISM1 antibodies and subjected to Western blotting with anti-ISM1 and anti-FLAG antibodies. **(D)** Mapping of ACVR1B^{ECD}-interacting domain of ISM1. HEK293T cells transiently expressing ACVR1B^{ECD} were cotransfected with wild-type ISM1 or domain-deleted ISM1 mutants. ACVR2B^{ECD} were also cotransfected with ACVR1B^{ECD} to potentially improve the interaction between ISM1 and ACVR1B^{ECD}. CM samples were immunoprecipitated with anti-ISM1 antibodies and immunoblotted with anti-HA antibodies. ISM1 interaction with ACVR1B^{ECD} is no longer observed when AMOP domain is absent. **(E)** Western blot of pSMAD2 in WCL of P19C6 cells treated with 100 ng/ml NODAL in the presence of mock, HIS-CER1, FLAG-LEFTY1, wild-type ISM1, ΔTSR1-ISM1, or ΔAMOP-ISM1 CM. Western blots for HIS (CER1), FLAG (LEFTY1), and ISM1 in CM samples is shown.

Discussion

ISM1 is the founding member of a new family of proteins whose function remains largely elusive. Based on its spatiotemporal distribution throughout mouse ontogeny, we suggested that ISM1 plays roles other than as an angiogenesis inhibitor (Osório et al., 2014). In the present work, for the first time, we reveal

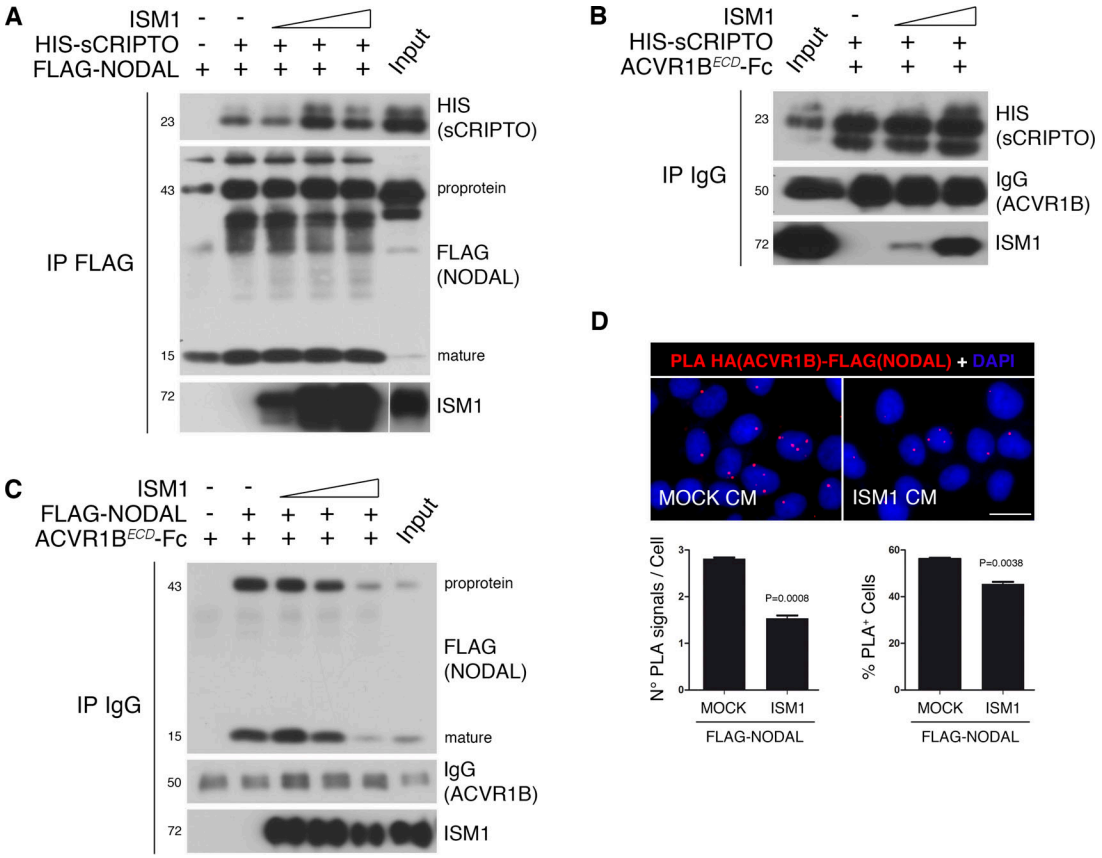

Figure 7. **ISM1 compromises formation of NODAL–ACVR1B complexes. (A)** A mix of FLAG-NODAL CM and HIS-sCRIPTO (soluble form of CRIPTO containing its extracellular domain) CM was incubated with increasing concentrations of ISM1 CM. The mixed CM samples were immunoprecipitated (IP) with anti-FLAG antibodies and analyzed by Western blot with antibodies against HIS, FLAG, and ISM1. **(B)** HIS-sCRIPTO CM and ACRV1B^{ECD}-Fc CM were mixed with increasing concentrations of ISM1 CM. Protein G agarose beads were used to precipitate the ACRV1B^{ECD}-Fc complexes, followed by Western blotting with the antibodies against HIS, IgG, and ISM1. **(C)** FLAG-NODAL CM and ACRV1B^{ECD}-Fc CM were incubated together in the presence of increasing concentrations of ISM1 CM before immunoprecipitation with protein G agarose beads. The precipitates were immunoblotted with antibodies against FLAG, IgG, and ISM1. **(D)** In situ PLA to detect the NODAL–ACVR1B complexes (red dots) in HeLa cells transiently expressing a low dose of ACVR1B-HA plasmid and treated with FLAG-NODAL CM in the presence of either mock or ISM1 CM. Cells were counterstained with DAPI to visualize nuclei. The number of PLA signals per cell (lower left) and the percentage of cells that have PLA signals (lower right) were counted in a total of 200 cells. Scale bars, 20 µm. Data represent mean ± SEM. The unpaired, two-tailed *t* test was used for statistical analyses.

that mouse ISM1 is a secretary protein with posttranslational modifications. We provide evidence that ISM1 is an *N*-glycosylated protein in which complex glycans are linked to the asparagine residues 39 and 282. We found that either point mutations at these residues or tunicamycin treatment abolished the secretion of ISM1. This observation indicates that caution should be taken when interpreting previous findings in functional studies on ISM1 produced in *Escherichia coli* lacking *N*-glycosylation. Our results also suggest that ISM1 is likely to carry other types of posttranslational modifications, as its molecular weight is still larger than expected even when *N*-glycosylation is abolished. Particularly, *O*-fucosylation as well as *C*-mannosylation have been identified within the TSR1 domain of several proteins (Hofsteenge et al., 2001; Luo et al., 2006) and were also predicted to occur in ISM1 (Du et al., 2010), though not yet experimentally validated.

Given limited information available, we searched for cues of potential putative functions of ISM1 based on its structural features. The presence of the TSR1 domain in ISM1 suggested the potential involvement of ISM1 in TGF-β superfamily signaling. To test this hypothesis, we analyzed if ISM1 affects the response of cells to TGF-β, ACTIVIN, and NODAL as well as BMP. We found that ISM1 modulates SMAD-mediated TGF-β superfamily signaling in a ligand-dependent manner. While ISM1 causes no alteration in signaling induced by TGF-β1, ACTIVIN, or BMP4, it specifically inhibits pSMAD2 induced by NODAL and its related member GDF1. This observation is consistent with previous reports showing that NODAL-GDF1 heterodimers rather than NODAL homodimers are required for NODAL signaling (Tanaka et al., 2007; Fuerer et al., 2014; Montague and Schier, 2017). These data identified ISM1 as a new extracellular antagonist of the NODAL signaling pathway. In ligand-binding assays, although ISM1 did not interact with the extracellular domain of ACVR2B, one of the NODAL receptors, or the transmembrane coreceptor CRIPTO, it bound to NODAL ligand and two other NODAL receptors, ACVR1B and ACVR2A (Figs. 5, S1, and S2). Although ISM1 interacted with ACVR2A, it did not interfere with the association between NODAL ligand and ACVR2A (Fig. S3).

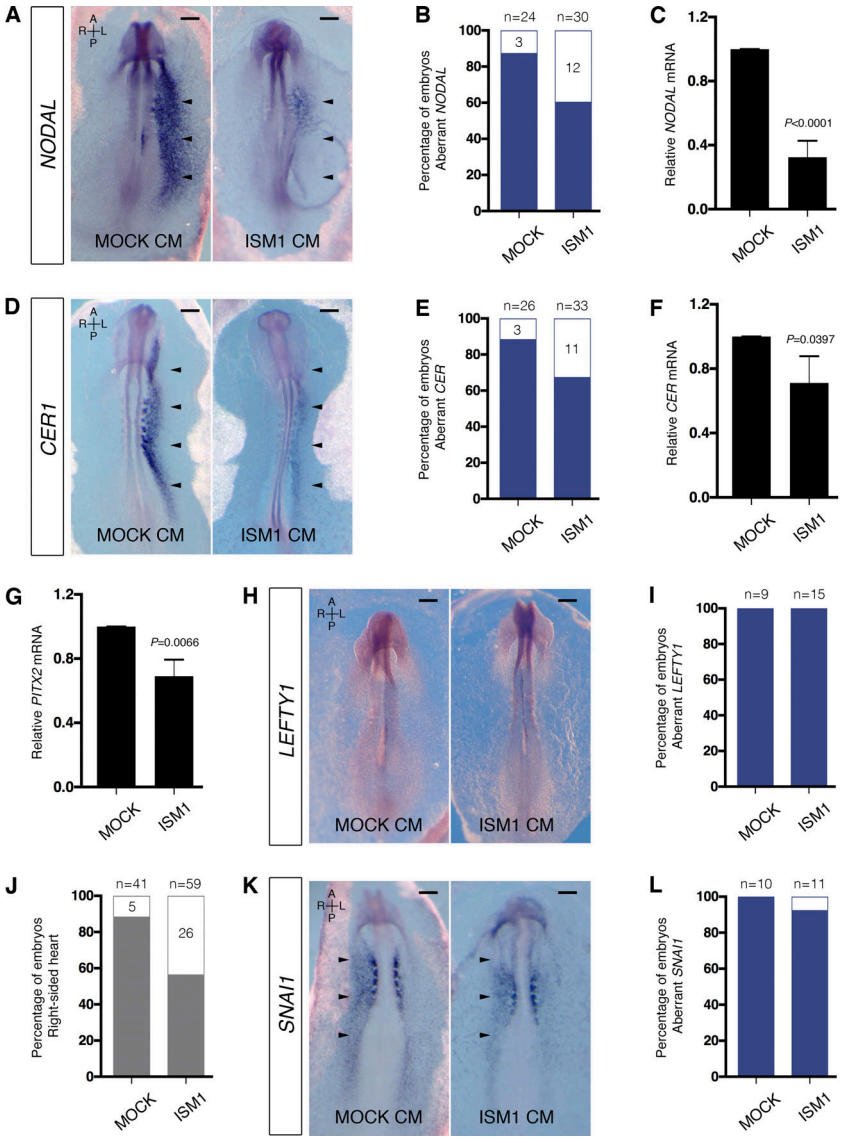

Figure 8. **Inhibition of NODAL signaling by ISM1 leads to defects in LR patterning in the chick embryo. (A)** *NODAL* whole-mount in situ hybridization in *ex ovo* cultured chick embryos treated with mock or ISM1 CM. Arrowheads indicate *NODAL* expression in the left LPM. **(B)** Percentage of embryos with aberrant (reduced or absent) *NODAL* expression treated with either mock or ISM1 CM. **(C)** Relative *NODAL* transcription in the left half of embryos treated with mock or ISM1 CM determined by qPCR. **(D)** *CER1* whole-mount in situ hybridization in *ex ovo* cultured chick embryos treated with mock or ISM1 CM. Arrowheads indicate *CER1* expression in the left LPM. **(E)** Percentage of embryos showing reduced *CER1* expression in the presence or absence of ISM1 CM. **(F and G)** Relative levels of *CER1* (F) and *PITX2* (G) transcripts in the left half of embryos in the presence or absence of ISM1. **(H)** Whole-mount in situ hybridization of *LEFTY1* in *ex ovo* cultured chick embryos treated with mock or ISM1 CM. No obvious difference in *LEFTY1* expression along the embryonic midline was observed. **(I)** Percentage of embryos with aberrant *LEFTY1* expression after culture with mock or ISM1 CM. **(J)** Percentage of embryos showing a right-sided heart position after mock or ISM1 CM treatment. **(K)** *SNAI* whole-mount in situ hybridization in *ex ovo* cultured chick embryos treated with mock or ISM1 CM. Arrowheads indicate *SNAI* expression in the right LPM. **(L)** Percentage of embryos showing abnormal *SNAI1* expression in the presence or absence of ISM1. For qPCR analyses, 10–12 embryos were pooled together for RNA purification. Two independent biological replicates were included. Three replicates of qPCR reactions were performed for each independent sample. Data represent mean ± SEM. The unpaired, two-tailed *t* test was used for statistical analysis. Statistically significant P values are indicated. All the embryos are shown in ventral view, and orientation along the AP and LR axes is indicated. Scale bars, 25 µm.

However, through a series of competitive-binding assays, we revealed that ISM1 specifically compromised the association between NODAL and ACVR1B (Fig. 7). Hence, the way by which ISM1 suppresses NODAL signaling is distinct from other secretary antagonists, LEFTY and CER (Fig. 9). Similar to GDF1, GDF3 is also a coligand essential for NODAL signaling (Levine et al., 2009; Peterson et al., 2013; Pelliccia et al., 2017). It is unclear whether ISM1 interacts with GDF1/GDF3 and jeopardizes NODAL signaling through interfering with NODAL/GDF heterodimer formation. Unexpectedly, the inhibitory effect of ISM1 on NODAL signaling requires the presence of the AMOP domain but not the TSR1 domain. The TSR1 domain is involved in the activation and regulation of TGF-β signaling, among other functions, and has been shown to have antiangiogenic activity (Adams and Lawler, 2011). However, none of these functions can be attributed to the TSR1 domain in ISM1 (Xiang et al., 2011; present work). On the other hand, the interaction between ISM1 and the components of NODAL signaling is lost upon AMOP domain deletion. Consistently, the inhibition of NODAL-induced SMAD2 activation is abrogated in the absence of AMOP, an uncommon and rarely studied motif implicated in the regulation of tumor angiogenesis in ISM1 and MUC4 (Zhang et al., 2011; Tang et al., 2016). ISM1 function in endothelial cells has been described to be dependent on a KGD motif located in the C-terminal portion of AMOP, important for integrin interaction. Our findings provide evidence of a new function of AMOP domain in the regulation of NODAL signaling.

NODAL signaling is subject to tight spatiotemporal regulation, fundamental for homeostasis and tumorigenesis in not only embryogenesis but also the adult reproductive tissues (Shen, 2007; Park and Dufort, 2011; Park et al., 2012; Kirsammer et al., 2014). Secreted antagonists (DAN/CER and LEFTY, identified previously, and ISM1, described in this study) exhibited different magnitudes of inhibition on NODAL signaling. Although the method we employed in the study to compare the inhibitory strength of three NODAL antagonists has limitations and is not quantitative, it showed that LEFTY1 was the most potent inhibitor of NODAL signaling, whereas ISM1 exhibited a considerably weaker activity than LEFTY1 but similar or slightly higher inhibitory potential compared with CER1 (Fig. 4). The

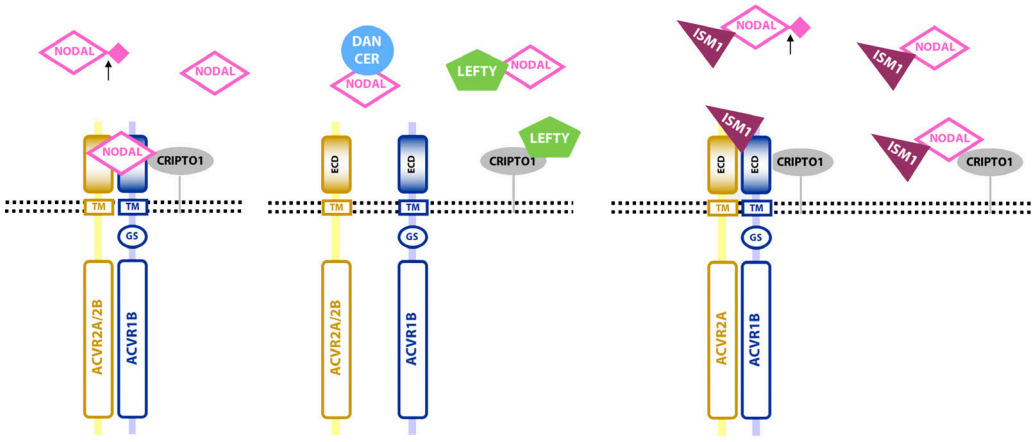

	DAN/CER	LEFTY	ISM1
NODAL *ligand*	Yes	Yes	Yes
***Co-receptor* CRIPTO1**	No	Yes	No
***Type I receptor* ACVR1B**	No	No	Yes
***Type II receptor* ACVR2A**	No	No	Yes
Inhibition	+	+++	++

Figure 9. **Working model for the inhibitory effect of ISM1 on NODAL signaling.** ISM1, a newly identified extracellular antagonist of NODAL signaling, interacts with both NODAL ligand and receptor complex ACVR2A–ACVR1B. ISM1 does not interact with CRIPTO but compromises the formation of NODAL–ACVR1B complex, therefore negatively regulating among DAN/CER, LEFTY1, and ISM1 on NODAL signaling as presented in the diagram. The table summarizes the binding profile of three NODAL antagonists with NODAL signaling components and their relative inhibitory strength.

difference in their inhibitory activities is likely attributable to the distinct underlying mechanisms through which NODAL signaling is regulated. CER1 uses a single mechanism, whereas LEFTY1 and ISM1 use distinct dual mechanisms (Fig. 9; Piccolo et al., 1999; Perea-Gomez et al., 2002; Chen and Shen, 2004; Cheng et al., 2004; Marques et al., 2004).

The differences in inhibition potentials and mechanisms used also seem to be in agreement with genetic studies in mice. Deletion of LEFTY genes in mice gives rise to phenotypes related to enhanced NODAL signaling, such as excess of mesoderm formation and defects in LR patterning (Meno et al., 1998, 1999). On the other hand, *Cer1* is not essential for mouse development, as *Cer1* knockout mice show no defects in anterior patterning and are fertile (Simpson et al., 1999; Belo et al., 2000; Stanley et al., 2000). The mild phenotypes observed in *Cer1* knockout mice may be attributable to the relatively mild inhibition of NODAL signaling, in addition to the proposed genetic compensation. Although a recent study reported that knockdown of *ISM1* in *Xenopus* resulted in craniofacial dysmorphologies, the potential link between the phenotype and nodal signaling was not investigated (Lansdon et al., 2018). In addition, the loss of *ISM1* may not significantly disturb NODAL signaling given that *LEFTY* genes have much stronger inhibitory effects on NODAL signaling. Whether loss- or gain-of-function in *Ism1* gene in mice will lead to phenotypes related to disturbed NODAL signaling remains to be determined. However, our analyses in *ex ovo* culture of chick embryos do support the biological relevance of ISM1 as an antagonist of NODAL signaling during embryonic development, as reduced signaling in left LPM and abnormal asymmetric heart morphogenesis were observed in the presence of ectopic ISM1 (Fig. 8). Although ISM1 may have other unidentified functions that contribute to these phenotypes, such as signaling pathways determining the right-side identity, our results do not support this possibility because of two lines of evidence. ISM1 has no effect on BMP signaling (Fig. 2 C), and ectopic ISM1 does not cause obvious changes in the expression of right-side marker *SNAI1* (Fig. 8, K and L).

ISM1 involvement in LR asymmetric organ morphogenesis was initially proposed because of its asymmetric expression in the anterior mesendoderm of E7.5 mouse embryos and the foregut endoderm of HH10 chicks (Osório et al., 2014). Data from the current study provide the first evidence of the involvement of ISM1 in the negative regulation of NODAL signaling during early embryogenesis. As ISM1 is expressed in several adult tissues, it is expected that ISM1 has additional roles in development yet to be explored. Taken together, our results reveal a novel regulatory paradigm for NODAL signaling, providing evidence of the complexity and plasticity in the fine-tuning of NODAL signaling by the combinatory effects of secretory antagonists. Our study sheds light on the molecular mechanism underlying NODAL signaling–mediated developmental processes as well as tumorigenesis.

Materials and methods

Cell culture and CM preparation

HEK293T and HeLa cells were maintained in DMEM (12100-046; Gibco) containing 10% FBS under 37°C and humidified 5% CO_2

conditions. P19C6 cells were maintained in DMEM/F12 medium with 10% FBS. HEK293T-CRIPTO cells are HEK293T cells stably expressing CRIPTO. FLAG-CRIPTO expression plasmid was transfected into HEK293T cells using Lipofectamine 2000 (11668-500; Invitrogen) according to the manufacturer's protocol. After selection of expressing clones, HEK293T-CRIPTO cells were maintained in DMEM containing 10% FBS and 750 µg/ml of Geneticin (10131-027; Gibco).

For CM preparation, the plasmids encoding the proteins of interest were transiently transfected into HEK293T cells. After transfection, cells were washed with PBS and the medium was changed to serum-free DMEM. CM samples were collected after 36 h and centrifuged at 4,000 rpm at 4°C before further usage/analysis.

Growth factor stimulations

HEK293T-CRIPTO or HEK293T cells were grown to 80–90% and serum starved for 12 h before stimulation with 40 ng/ml TGF-β1 (100-B; R&D Systems), 100 ng/ml NODAL (1315-ND/CF; R&D Systems), 100 ng/ml GDF1 (6937-GD/CF; R&D Systems), 40 ng/ml ACTIVIN-A (338-AC; R&D Systems), or 50 ng/ml BMP4 (314-BP; R&D Systems) in the presence of CM as indicated. Mouse rISM1 (577502; BioLegend) was used at 100 or 200 ng/ml. CM were preincubated at 37°C for 30 min with gentle shaking before being added to the cells. For P19C6 cells, cells were grown to 60–80% and serum starved for 18 h followed by stimulation for 1 h with 100 ng/ml NODAL in the presence of prewarmed CM as indicated.

Plasmid vectors

Mouse ISM1 cDNA plasmids were prepared as described previously (Osório et al., 2014). Epitope-tagged and chimeric constructs were generated by PCR-based strategy, and domain deletions and amino acid substitution by site-directed mutagenesis. Positive clones were confirmed by restriction enzyme and sequencing analyses. In FLAG-NODAL, the FLAG epitope was introduced 4 amino acids downstream of the proteolytic cleavage site of the NODAL proprotein. ACVR1B-HA was generated by fusion of the HA epitope to the C terminus of the mouse ACVR1B cDNA sequence. ACVR1B^{ECD}-HA contains the cDNA encoding amino acids 1–126 (ECD) of ACVR1B fused to the HA epitope. Chimeric ACVR1B^{ECD}-Fc receptor was generated by cloning the cDNA encoding amino acids 1–126 of ACVR1B fused in-frame with the human IgG Fc fragment derived from pRK5-mFz8CRD-IgG (Semënov et al., 2001; 16689 Plasmid; Addgene; from Dr. Xi He, Harvard Medical School, Boston, MA). ACVR2B^{ECD}-MYC was obtained by fusion of the cDNA corresponding to amino acids 1–134 (ECD) of mouse ACVR2B to the MYC epitope. MYC-ACVR2A and CER1-FLAG plasmids were purchased from Sino Biological (MG50613-NM and MG51161-CF, respectively). HIS-sCRIPTO was obtained by amplification of CRIPTO cDNA corresponding to amino acids 1–150 (lacking the GPI motif) and tagged with HIS epitope. A list of the primers used is available in Table S1. Plasmid pcDNA3-FLAG-LEFTY1 was a kind gift from Dr. Michael Shen (Robert Wood Johnson Medical School, New Brunswick, NJ; Chen and Shen, 2004). pFLAG-CMV1-ISM1 mammalian-expressing plasmid was subcloned using HindIII/EcoRI from pcDNA3-ISM1 plasmid into pFLAG-CMV-1 vector (E7273; Sigma-Aldrich).

N-glycosylation modification assay

WCL and CM were obtained from HEK293T cells transiently transfected with mock, ISM1, N39Q, N282Q, N39Q/N282Q, ΔTSR1, or ΔAMOP. According to the manufacturer's instructions, the samples were treated with PNGase F (P0704S; New England Biolabs) or Endo H (P0702S; New England Biolabs) and analyzed by Western blotting. For tunicamycin treatment, transfected cells were treated with 1 ng/ml tunicamycin (654380; Calbiochem) for 8 h before harvesting.

Protein extraction and Western blotting

Cells were lysed in radioimmunoprecipitation assay buffer containing a protease inhibitor cocktail (11836145001; Roche) and sodium orthovanate. The protein concentration was determined using DC Protein Assay (500-0111; Bio-Rad), and 15–30 µg of total protein lysates were used. Samples were resolved by SDS-PAGE under reducing conditions and blotted onto a polyvinylidene fluoride membrane (03010040001; Roche). Membranes were probed with specific primary antibodies followed by peroxidase-conjugated secondary antibodies. The bands were detected using SuperSignal West Pico Chemiluminescent Substrate (1859674; Thermo Fisher Scientific) according to the manufacturer's protocol. Densitometry analyses were performed using the ImageJ program (http://imagej.nih.gov/ij/), and the quantification results were normalized to the loading control. The following primary antibodies were used: mouse anti–β-actin (1:5,000, A5316; Sigma-Aldrich), mouse anti-FLAG (1:2,000, F1804; Sigma-Aldrich), mouse anti-HA (1:1,000, MMS-101P; Covance), rabbit anti-HIS (1:1,000, sc-803; Santa Cruz Biotechnology), goat anti-IgG (Fc; 1:2,000, 109-035-008; Jackson ImmunoResearch), rabbit anti-ISM1 (1:5,000, Genescript; Osório et al., 2014), mouse anti-MYC (1:1,000, sc-40; Santa Cruz Biotechnology), mouse anti-SMAD2/3 (1:2,000, 610845; BD Transduction Laboratories), rabbit anti-pSMAD2 (1:1,000, 3101; Cell Signaling), and mouse anti-GST (1:3,000, sc-138; Santa Cruz Biotechnology). The secondary antibodies used were HRP-conjugated rabbit anti-goat IgG (1:3,000, 81-1620; Invitrogen), HRP-conjugated rabbit anti-mouse IgG (1:3,000, 64-6420; Invitrogen), and HRP-conjugated goat anti-rabbit IgG (1:3,000, 65-6120; Invitrogen).

Dual luciferase reporter assay

HEK293T-CRIPTO cells were cotransfected with plasmids encoding A3-*lux* firefly reporter, FLAG-FOXH1, and RS-SV40 renilla reporter and serum starved for 12 h before stimulation with 100 ng/ml NODAL, 100 ng/ml GDF1, 40 ng/ml ACTIVIN-A, and 40 ng/ml TGF-β1 for 18–24 h. The CM were preincubated at 37°C for 30 min with gentle shaking before being added to the cells. Dual luciferase reporter assay was performed following the manufacturer's instructions (E1960; Promega). A3-*lux* firefly reporter, FLAG-FOXH1, and RS-SV40 renilla reporter plasmids were a kind gift from Dr. Michael Shen (Chen and Shen, 2004). *A3-luc* contains three copies of the ACTIVIN-NODAL-TGF-β responsive element of the well-known SMAD2 target *Mix.2* promoter.

Immunoprecipitation and competitive binding assays

CM harvested from HEK293T cells transiently transfected with the different plasmids were used. Briefly, CM were incubated with appropriate antibodies at 4°C for 2 h. Protein A agarose (11134515001; Roche) or protein G agarose (11243233001; Roche) beads were then added, and the protein/antibody/bead complexes were incubated at 4°C overnight. ACVR1B^{ECD}-Fc complexes were precipitated with protein G agarose with no antibody. After washing with lysis buffer, the complexes were eluted by boiling with 2× SDS loading buffer and analyzed by immunoblotting. For competitive binding assays, the CM harvested from transiently transfected cells were mixed, incubated at room temperature for 1 h with gentle shaking, and then subjected to immunoprecipitation.

In situ PLAs

HeLa cells were transfected with ACVR1B-HA for 8 h and serum starved for 12 h. CM were preincubated at 37°C for 30 min with gentle shaking before being added to the cells as indicated. The cells were fixed in 4% PFA for 10 min and then processed for PLA using Duolink II Red Starter Kit (92101; OLink) according to the manufacturer's instructions. Cells were counterstained with DAPI (D1306; Molecular Probes), mounted with SlowFade Gold antifade reagent (S36936; Molecular Probes), and photographed using an Olympus BX51 microscope equipped with a Spot RT3 charge-coupled device camera. Images and figures were processed with Adobe Photoshop CS5. For each experimental group, the number of PLA signals was counted in a total of 200 cells.

Chick embryos and *ex ovo* culture

Fertilized chick eggs were obtained from Jinan Poultry Co. (Tin Hang Technology) and incubated in a humidified atmosphere. Embryos were staged according to the table in Hamburger and Hamilton (1951). For the experiments using CM, whole embryos at HH4–5 were cultured *ex ovo* using the easy culture method as previously described (Chapman et al., 2001). Briefly, the embryos were cultured ventral-side up on top of a 20-µl drop of CM placed on the semisolid agar-albumin substrate. Another 20 µl of CM were gently placed on top of the embryo. For the beads experiment, embryos at HH4 or HH6 were cultured using the new culture method as reported (Alev et al., 2013). 2 µl of PBS-washed heparin-acrylic beads (H5262; Sigma-Aldrich) were soaked in 2.5 µl of rNODAL mixed with either 2.5 µl PBS or 2.5 µl rISM1 (577502; BioLegend) for ∼3 h on ice. Before implantation, the beads were washed three times in Pannett–Compton solution. For both experiments, the embryos were incubated until they reached stages HH7–9 or HH10–12 and processed for whole-mount in situ hybridization and/or qPCR analyses. Embryos exhibiting gross morphological defects were equally excluded from control and experimental groups and not considered in further analysis.

Whole-mount in situ hybridization

RNA probes for in situ hybridization were prepared by in vitro transcription as previously described (Osório et al., 2014). Briefly, plasmids were linearized, purified by phenol-chloroform, and used as template for the transcription reaction containing digoxigenin (DIG) RNA Labeling Mix (11277073910; Roche). RQ1 DNase I (M6101; Promega) was used to remove the excess of template DNA. DIG-labeled RNA was purified by ProbeQuant G-50 Micro Columns (28-9034-08; GE Healthcare). Whole-mount in situ hybridization in young embryos was performed as described (Streit and Stern, 2001). In short, the fixed embryos were treated with methanol and proteinase K and postfixed. The embryos were then prehybridized for 3 h before incubation with DIG-labeled probes overnight at 68°C. After extensive washing, the embryos were blocked in 5% goat serum and 1 mg/ml BSA and then incubated with sheep anti-DIG-AP antibody (11093274910; Roche) overnight at 4°C. AP activity was detected using nitro blue tetrazolium and 5-bromo-4-chloro-3-indolyl phosphate substrate. Once color developed, the embryos were washed and fixed. Whole-mount embryos were photographed on a Leica MZ10F stereomicroscope coupled with a Leica DFC310FX camera. Images and figures were processed with Adobe Photoshop CS5. For histological analyses, the fixed embryos were incubated in 15% sucrose overnight at 4°C, embedded in gelatin, frozen, and serially sectioned on a Leica CM3050S cryostat. Sections were photographed using an Olympus BX51 microscope equipped with a Spot RT3 CCD camera. Images and figures were processed with Adobe Photoshop CS5.

RNA extraction and qPCR analyses

Embryos cultured until HH7–9 were dissected along the midline, and the extracellular embryonic tissues were removed. 10–12 embryos were used per group. The left half of the embryos were mixed together and processed for total RNA extraction using Trizol (15596-026; Invitrogen) according to the manufacturer's instructions. RQ1 DNase I was used to eliminate genomic DNA contamination from the RNA samples before synthesis of first-strand cDNA. Briefly, 2 µg of total RNA was reverse transcribed using Oligo(dT)$_{15}$ primer (C1101; Promega) and Moloney murine leukemia virus reverse transcription (M170; Promega). Real-time PCR was performed on a StepOne PCR machine (Applied Biosystems) using Power SYBR Green PCR Master Mix (4368577; Applied Biosystems). All absolute data were first normalized to 18S RNA and then normalized to the control sample treated with mock CM. The relative transcriptional levels of the genes were determined by the ΔΔCt method. Two biological experiments were included, and for each, two independent PCR reactions with three replicates each were performed. The sequences of the primers used are listed in Table S2.

Statistical analysis

For all experiments, no statistical method was used to predetermine size sample, and investigators were not blinded to allocation during experiments and outcome assessment. Statistical analysis was performed using Prism 6 software (GraphPad). The data are represented as mean ± SEM, and unpaired, two-tailed Student's *t* test was used to compare two groups of individual samples. The data analyzed meet normal distribution, and an *F* test showed that variances were not significantly different between groups. Statistically significant P values are indicated.

Online supplemental material

Fig. S1 shows that ISM1 directly interacts with NODAL and ACVR1B by GST pull-down and SPR assays. Fig. S2 shows that ISM1 interacts with type II receptor ACVR2A. Fig. S3 shows that ISM1 did not intervene in the interaction between NODAL and ACVR2A. Table S1 describes the primers used for generation of the different constructs for mammalian expression. Table S2 describes the primers used in qPCR.

Acknowledgments

We thank Michael Shen, Dong-Yan Jin, Julian Tanner, Marian Ros, and Thomas Brand for plasmids and Naihe Jing for P19C6 cells. We also thank Patrick Tam and Robin Lovell-Badge for their discussions and comments.

This work is supported by Hong Kong General Research Fund (HKU 787011M), the University of Hong Kong Committee on Research and Conference Grants (CRCG) Small Funding Project (HKU 201001176085), National Science Foundation of China, and Health and Medical Research Fund grants.

The authors declare no competing financial interests.

Author contributions: Z. Zhou conceived and supervised the project. X. Wu, L. Osório, L. Wang, and Z. Jiang designed, performed, and analyzed the experiments. C. Neideck helped to perform experiments on Activin-A and TGF-β1 signaling. G. Sheng advised on design and execution of the chick experiments. Z. Zhou, L. Wang, and L. Osório wrote the manuscript with input from the other authors.

Submitted: 12 January 2018
Revised: 24 March 2019
Accepted: 6 May 2019

References

Adams, J.C., and J. Lawler. 2011. The thrombospondins. *Cold Spring Harb. Perspect. Biol.* 3:a009712. https://doi.org/10.1101/cshperspect.a009712

Alev, C., Y. Wu, T. Kasukawa, L.M. Jakt, H.R. Ueda, and G. Sheng. 2010. Transcriptomic landscape of the primitive streak. *Development.* 137: 2863–2874. https://doi.org/10.1242/dev.053462

Alev, C., M. Nakano, Y. Wu, H. Horiuchi, and G. Sheng. 2013. Manipulating the avian epiblast and epiblast-derived stem cells. *Methods Mol. Biol.* 1074:151–173. https://doi.org/10.1007/978-1-62703-628-3_12

Belo, J.A., D. Bachiller, E. Agius, C. Kemp, A.C. Borges, S. Marques, S. Piccolo, and E.M. De Robertis. 2000. Cerberus-like is a secreted BMP and nodal antagonist not essential for mouse development. *Genesis.* 26:265–270. https://doi.org/10.1002/(SICI)1526-968X(200004)26:4<265::AID-GENE80>3.0.CO;2-4

Bennett, J.T., K. Joubin, S. Cheng, P. Aanstad, R. Herwig, M. Clark, H. Lehrach, and A.F. Schier. 2007. Nodal signaling activates differentiation genes during zebrafish gastrulation. *Dev. Biol.* 304:525–540. https://doi.org/10.1016/j.ydbio.2007.01.012

Branford, W.W., and H.J. Yost. 2002. Lefty-dependent inhibition of Nodal- and Wnt-responsive organizer gene expression is essential for normal gastrulation. *Curr. Biol.* 12:2136–2141. https://doi.org/10.1016/S0960-9822(02)01360-X

Chapman, S.C., J. Collignon, G.C. Schoenwolf, and A. Lumsden. 2001. Improved method for chick whole-embryo culture using a filter paper carrier. *Dev. Dyn.* 220:284–289. https://doi.org/10.1002/1097-0177(20010301)220:3<284::AID-DVDY1102>3.0.CO;2-5

Chen, C., and M.M. Shen. 2004. Two modes by which Lefty proteins inhibit nodal signaling. *Curr. Biol.* 14:618–624. https://doi.org/10.1016/j.cub.2004.02.042

Chen, M., Y. Zhang, V.C. Yu, Y.S. Chong, T. Yoshioka, and R. Ge. 2014. Isthmin targets cell-surface GRP78 and triggers apoptosis via induction of mitochondrial dysfunction. *Cell Death Differ.* 21:797–810. https://doi.org/10.1038/cdd.2014.3

Chen, X., M.J. Rubock, and M. Whitman. 1996. A transcriptional partner for MAD proteins in TGF-beta signalling. *Nature.* 383:691–696. https://doi.org/10.1038/383691a0

Chen, X., E. Weisberg, V. Fridmacher, M. Watanabe, G. Naco, and M. Whitman. 1997. Smad4 and FAST-1 in the assembly of activin-responsive factor. *Nature.* 389:85–89. https://doi.org/10.1038/38008

Cheng, S.K., F. Olale, A.H. Brivanlou, and A.F. Schier. 2004. Lefty blocks a subset of TGFbeta signals by antagonizing EGF-CFC coreceptors. *PLoS Biol.* 2:E30. https://doi.org/10.1371/journal.pbio.0020030

Ciccarelli, F.D., T. Doerks, and P. Bork. 2002. AMOP, a protein module alternatively spliced in cancer cells. *Trends Biochem. Sci.* 27:113–115. https://doi.org/10.1016/S0968-0004(01)02049-7

Collignon, J., I. Varlet, and E.J. Robertson. 1996. Relationship between asymmetric nodal expression and the direction of embryonic turning. *Nature.* 381:155–158. https://doi.org/10.1038/381155a0

Conlon, F.L., K.M. Lyons, N. Takaesu, K.S. Barth, A. Kispert, B. Herrmann, and E.J. Robertson. 1994. A primary requirement for nodal in the formation and maintenance of the primitive streak in the mouse. *Development.* 120:1919–1928.

Constam, D.B. 2014. Regulation of TGFβ and related signals by precursor processing. *Semin. Cell Dev. Biol.* 32:85–97. https://doi.org/10.1016/j.semcdb.2014.01.008

Du, J., H. Takeuchi, C. Leonhard-Melief, K.R. Shroyer, M. Dlugosz, R.S. Haltiwanger, and B.C. Holdener. 2010. O-fucosylation of thrombospondin type 1 repeats restricts epithelial to mesenchymal transition (EMT) and maintains epiblast pluripotency during mouse gastrulation. *Dev. Biol.* 346:25–38. https://doi.org/10.1016/j.ydbio.2010.07.008

Feldman, B., M.L. Concha, L. Saúde, M.J. Parsons, R.J. Adams, S.W. Wilson, and D.L. Stemple. 2002. Lefty antagonism of Squint is essential for normal gastrulation. *Curr. Biol.* 12:2129–2135. https://doi.org/10.1016/S0960-9822(02)01361-1

Fuerer, C., M.C. Nostro, and D.B. Constam. 2014. Nodal·Gdf1 heterodimers with bound prodomains enable serum-independent nodal signaling and endoderm differentiation. *J. Biol. Chem.* 289:17854–17871. https://doi.org/10.1074/jbc.M114.550301

Gray, P.C., C.A. Harrison, and W. Vale. 2003. Cripto forms a complex with activin and type II activin receptors and can block activin signaling. *Proc. Natl. Acad. Sci. USA.* 100:5193–5198. https://doi.org/10.1073/pnas.0531290100

Grimes, D.T., and R.D. Burdine. 2017. Left-Right Patterning: Breaking Symmetry to Asymmetric Morphogenesis. *Trends Genet.* 33:616–628. https://doi.org/10.1016/j.tig.2017.06.004

Hamburger, V., and H.L. Hamilton. 1951. A series of normal stages in the development of the chick embryo. *J. Morphol.* 88:49–92. https://doi.org/10.1002/jmor.1050880104

Hofsteenge, J., K.G. Huwiler, B. Macek, D. Hess, J. Lawler, D.F. Mosher, and J. Peter-Katalinic. 2001. C-mannosylation and O-fucosylation of the thrombospondin type 1 module. *J. Biol. Chem.* 276:6485–6498. https://doi.org/10.1074/jbc.M008073200

Iratni, R., Y.T. Yan, C. Chen, J. Ding, Y. Zhang, S.M. Price, D. Reinberg, and M.M. Shen. 2002. Inhibition of excess nodal signaling during mouse gastrulation by the transcriptional corepressor DRAP1. *Science.* 298: 1996–1999. https://doi.org/10.1126/science.1073405

Kelber, J.A., G. Shani, E.C. Booker, W.W. Vale, and P.C. Gray. 2008. Cripto is a noncompetitive activin antagonist that forms analogous signaling complexes with activin and nodal. *J. Biol. Chem.* 283:4490–4500. https://doi.org/10.1074/jbc.M704960200

Kirsammer, G., L. Strizzi, N.V. Margaryan, A. Gilgur, M. Hyser, J. Atkinson, D.A. Kirschmann, E.A. Seftor, and M.J. Hendrix. 2014. Nodal signaling promotes a tumorigenic phenotype in human breast cancer. *Semin. Cancer Biol.* 29:40–50. https://doi.org/10.1016/j.semcancer.2014.07.007

Lansdon, L.A., B.W. Darbro, A.L. Petrin, A.M. Hulstrand, J.M. Standley, R.B. Brouillette, A. Long, M.A. Mansilla, R.A. Cornell, J.C. Murray, et al. 2018. Identification of *Isthmin 1* as a Novel Clefting and Craniofacial Patterning Gene in Humans. *Genetics.* 208:283–296. https://doi.org/10.1534/genetics.117.300535

Levine, A.J., Z.J. Levine, and A.H. Brivanlou. 2009. GDF3 is a BMP inhibitor that can activate Nodal signaling only at very high doses. *Dev. Biol.* 325: 43–48. https://doi.org/10.1016/j.ydbio.2008.09.006

Liu, F., C. Pouponnot, and J. Massagué. 1997. Dual role of the Smad4/DPC4 tumor suppressor in TGFbeta-inducible transcriptional complexes. *Genes Dev.* 11:3157–3167. https://doi.org/10.1101/gad.11.23.3157

Luo, Y., A. Nita-Lazar, and R.S. Haltiwanger. 2006. Two distinct pathways for O-fucosylation of epidermal growth factor-like or thrombospondin type

1 repeats. *J. Biol. Chem.* 281:9385–9392. https://doi.org/10.1074/jbc.M511974200

Marques, S., A.C. Borges, A.C. Silva, S. Freitas, M. Cordenonsi, and J.A. Belo. 2004. The activity of the Nodal antagonist Cerl-2 in the mouse node is required for correct L/R body axis. *Genes Dev.* 18:2342–2347. https://doi.org/10.1101/gad.306504

Meno, C., A. Shimono, Y. Saijoh, K. Yashiro, K. Mochida, S. Ohishi, S. Noji, H. Kondoh, and H. Hamada. 1998. lefty-1 is required for left-right determination as a regulator of lefty-2 and nodal. *Cell.* 94:287–297. https://doi.org/10.1016/S0092-8674(00)81472-5

Meno, C., K. Gritsman, S. Ohishi, Y. Ohfuji, E. Heckscher, K. Mochida, A. Shimono, H. Kondoh, W.S. Talbot, E.J. Robertson, et al. 1999. Mouse Lefty2 and zebrafish antivin are feedback inhibitors of nodal signaling during vertebrate gastrulation. *Mol. Cell.* 4:287–298. https://doi.org/10.1016/S1097-2765(00)80331-7

Montague, T.G., and A.F. Schier. 2017. Vg1-Nodal heterodimers are the endogenous inducers of mesendoderm. *eLife.* 6:e28183. https://doi.org/10.7554/eLife.28183

Moremen, K.W., M. Tiemeyer, and A.V. Nairn. 2012. Vertebrate protein glycosylation: diversity, synthesis and function. *Nat. Rev. Mol. Cell Biol.* 13:448–462. https://doi.org/10.1038/nrm3383

Nakamura, T., and H. Hamada. 2012. Left-right patterning: conserved and divergent mechanisms. *Development.* 139:3257–3262. https://doi.org/10.1242/dev.061606

Ocaña, O.H., H. Coskun, C. Minguillón, P. Murawala, E.M. Tanaka, J. Galcerán, R. Muñoz-Chápuli, and M.A. Nieto. 2017. A right-handed signalling pathway drives heart looping in vertebrates. *Nature.* 549:86–90. https://doi.org/10.1038/nature23454

Osório, L., X. Wu, and Z. Zhou. 2014. Distinct spatiotemporal expression of ISM1 during mouse and chick development. *Cell Cycle.* 13:1571–1582. https://doi.org/10.4161/cc.28494

Park, C.B., and D. Dufort. 2011. Nodal expression in the uterus of the mouse is regulated by the embryo and correlates with implantation. *Biol. Reprod.* 84:1103–1110. https://doi.org/10.1095/biolreprod.110.087239

Park, C.B., F.J. DeMayo, J.P. Lydon, and D. Dufort. 2012. NODAL in the uterus is necessary for proper placental development and maintenance of pregnancy. *Biol. Reprod.* 86:194. https://doi.org/10.1095/biolreprod.111.098277

Pelliccia, J.L., G.A. Jindal, and R.D. Burdine. 2017. Gdf3 is required for robust Nodal signaling during germ layer formation and left-right patterning. *eLife.* 6:e28635. https://doi.org/10.7554/eLife.28635

Pera, E.M., J.I. Kim, S.L. Martinez, M. Brechner, S.Y. Li, O. Wessely, and E.M. De Robertis. 2002. Isthmin is a novel secreted protein expressed as part of the Fgf-8 synexpression group in the Xenopus midbrain-hindbrain organizer. *Mech. Dev.* 116:169–172. https://doi.org/10.1016/S0925-4773(02)00123-5

Perea-Gomez, A., F.D. Vella, W. Shawlot, M. Oulad-Abdelghani, C. Chazaud, C. Meno, V. Pfister, L. Chen, E. Robertson, H. Hamada, et al. 2002. Nodal antagonists in the anterior visceral endoderm prevent the formation of multiple primitive streaks. *Dev. Cell.* 3:745–756. https://doi.org/10.1016/S1534-5807(02)00321-0

Peterson, A.G., X. Wang, and H.J. Yost. 2013. Dvr1 transfers left-right asymmetric signals from Kupffer's vesicle to lateral plate mesoderm in zebrafish. *Dev. Biol.* 382:198–208. https://doi.org/10.1016/j.ydbio.2013.06.011

Piccolo, S., E. Agius, L. Leyns, S. Bhattacharyya, H. Grunz, T. Bouwmeester, and E.M. De Robertis. 1999. The head inducer Cerberus is a multifunctional antagonist of Nodal, BMP and Wnt signals. *Nature.* 397:707–710. https://doi.org/10.1038/17820

Rossant, J., and P.P. Tam. 2009. Blastocyst lineage formation, early embryonic asymmetries and axis patterning in the mouse. *Development.* 136:701–713. https://doi.org/10.1242/dev.017178

Schier, A.F. 2009. Nodal morphogens. *Cold Spring Harb. Perspect. Biol.* 1:a003459. https://doi.org/10.1101/cshperspect.a003459

Schlueter, J., and T. Brand. 2009. A right-sided pathway involving FGF8/Snai1 controls asymmetric development of the proepicardium in the chick embryo. *Proc. Natl. Acad. Sci. USA.* 106:7485–7490. https://doi.org/10.1073/pnas.0811944106

Semënov, M.V., K. Tamai, B.K. Brott, M. Kühl, S. Sokol, and X. He. 2001. Head inducer Dickkopf-1 is a ligand for Wnt coreceptor LRP6. *Curr. Biol.* 11:951–961. https://doi.org/10.1016/S0960-9822(01)00290-1

Shen, M.M. 2007. Nodal signaling: developmental roles and regulation. *Development.* 134:1023–1034. https://doi.org/10.1242/dev.000166

Simpson, E.H., D.K. Johnson, P. Hunsicker, R. Suffolk, S.A. Jordan, and I.J. Jackson. 1999. The mouse Cer1 (Cerberus related or homologue) gene is not required for anterior pattern formation. *Dev. Biol.* 213:202–206. https://doi.org/10.1006/dbio.1999.9372

Smith, K.A., E. Noël, I. Thurlings, H. Rehmann, S. Chocron, and J. Bakkers. 2011. Bmp and nodal independently regulate lefty1 expression to maintain unilateral nodal activity during left-right axis specification in zebrafish. *PLoS Genet.* 7:e1002289. https://doi.org/10.1371/journal.pgen.1002289

Stanley, E.G., C. Biben, J. Allison, L. Hartley, I.P. Wicks, I.K. Campbell, M. McKinley, L. Barnett, F. Koentgen, L. Robb, and R.P. Harvey. 2000. Targeted insertion of a lacZ reporter gene into the mouse Cer1 locus reveals complex and dynamic expression during embryogenesis. *Genesis.* 26:259–264. https://doi.org/10.1002/(SICI)1526-968X(200004)26:4<259::AID-GENE70>3.0.CO;2-V

Streit, A., and C.D. Stern. 2001. Combined whole-mount in situ hybridization and immunohistochemistry in avian embryos. *Methods.* 23:339–344. https://doi.org/10.1006/meth.2000.1146

Tanaka, C., R. Sakuma, T. Nakamura, H. Hamada, and Y. Saijoh. 2007. Long-range action of Nodal requires interaction with GDF1. *Genes Dev.* 21:3272–3282. https://doi.org/10.1101/gad.1623907

Tang, J., Y. Zhu, K. Xie, X. Zhang, X. Zhi, W. Wang, Z. Li, Q. Zhang, L. Wang, J. Wang, and Z. Xu. 2016. The role of the AMOP domain in MUC4/Y-promoted tumour angiogenesis and metastasis in pancreatic cancer. *J. Exp. Clin. Cancer Res.* 35:91. https://doi.org/10.1186/s13046-016-0369-0

Tucker, R.P. 2004. The thrombospondin type 1 repeat superfamily. *Int. J. Biochem. Cell Biol.* 36:969–974. https://doi.org/10.1016/j.biocel.2003.12.011

Wakefield, L.M., and C.S. Hill. 2013. Beyond TGFβ: roles of other TGFβ superfamily members in cancer. *Nat. Rev. Cancer.* 13:328–341. https://doi.org/10.1038/nrc3500

Wang, Y., X. Wang, T. Wohland, and K. Sampath. 2016. Extracellular interactions and ligand degradation shape the nodal morphogen gradient. *eLife.* 5:e13879. https://doi.org/10.7554/eLife.13879

Weidinger, G., C.J. Thorpe, K. Wuennenberg-Stapleton, J. Ngai, and R.T. Moon. 2005. The Sp1-related transcription factors sp5 and sp5-like act downstream of Wnt/beta-catenin signaling in mesoderm and neuroectoderm patterning. *Curr. Biol.* 15:489–500. https://doi.org/10.1016/j.cub.2005.01.041

Xiang, W., Z. Ke, Y. Zhang, G.H. Cheng, I.D. Irwan, K.N. Sulochana, P. Potturi, Z. Wang, H. Yang, J. Wang, et al. 2011. Isthmin is a novel secreted angiogenesis inhibitor that inhibits tumour growth in mice. *J. Cell. Mol. Med.* 15:359–374. https://doi.org/10.1111/j.1582-4934.2009.00961.x

Yamamoto, M., N. Mine, K. Mochida, Y. Sakai, Y. Saijoh, C. Meno, and H. Hamada. 2003. Nodal signaling induces the midline barrier by activating Nodal expression in the lateral plate. *Development.* 130:1795–1804. https://doi.org/10.1242/dev.00408

Yan, Y.T., J.J. Liu, Y. Luo, C. E, R.S. Haltiwanger, C. Abate-Shen, and M.M. Shen. 2002. Dual roles of Cripto as a ligand and coreceptor in the nodal signaling pathway. *Mol. Cell. Biol.* 22:4439–4449. https://doi.org/10.1128/MCB.22.13.4439-4449.2002

Zhang, Y., M. Chen, S. Venugopal, Y. Zhou, W. Xiang, Y.H. Li, Q. Lin, R.M. Kini, Y.S. Chong, and R. Ge. 2011. Isthmin exerts pro-survival and death-promoting effect on endothelial cells through alphavbeta5 integrin depending on its physical state. *Cell Death Dis.* 2:e153. https://doi.org/10.1038/cddis.2011.37

Zhou, X., H. Sasaki, L. Lowe, B.L. Hogan, and M.R. Kuehn. 1993. Nodal is a novel TGF-beta-like gene expressed in the mouse node during gastrulation. *Nature.* 361:543–547. https://doi.org/10.1038/361543a0